Effects of Adhesive Characteristics between Matrix and Reinforced Nanoparticle of AA6061/Carbon Black Nanocomposites

T. Prasad, A. Chennakesava Reddy

Abstract— This paper presents the experimental and finite element analysis of AA6061/carbon black nanocomposites. A cubical representative volume element (RVE) has been implemented to analyze the tensile behavior AA6061/carbon black nanocomposites. The carbon black nanoparticles were randomly distributed in the AA6061 matrix. The tensile strength was increased with an increase of carbon black content in the nanocomposites. The interfacial debonding was high between the particle and the matrix because the local stress concentration around the nanoparticle was increased with an increase in the volume fraction of carbon black in the nanocomposite.

Index Terms— AA6061, carbon black, RVE model, strengthening mechanism, FEA.

1 Introduction

THE higher stiffness of ceramic particles can lead to the incremental increase of a composite's stiffness [1, 2]. Micron-sized particles usually cause a reduction in impact resistance. On the other hand, using nanoparticles can lead to better impact and wear performance [3]. The existence of an interphase region with a higher strength and modulus than the polymer matrix would cause the composites to have superior mechanical properties [4]. Decreasing the interfacial strength can cause the interfacial debonding of particles from the matrix. Interfacial debonding can cause shear yielding of the matrix around the particles. Very small particles are difficult to disperse, creating agglomerates that behave as a large, single particle [5, 6]. The tensile properties of nanocomposites, including their tensile strength and elastic modulus, were analyzed via micromechanical models. The modulus magnitude depends on interfacial adhesion and the matrix's crystalline structure [7, 8].

AA6061 is a precipitation hardening aluminum alloy containing magnesium and silicon as its major alloying elements. AA6061 is commonly used for the construction of aircraft structures, such as wings and fuselages, automotive parts, such as wheel spacers and aluminum cans for the packaging of foodstuffs and beverages.

Carbon black is a material with high economic importance containing pure carbon. Carbon black is produced through specific combustion processes and the production of this material can be traced back more than one hundred years. It is used in many products including car tyres, printer toner, dyes for leather or textiles and mascara.

The aim of the present work is to fabricate the composites of AA6061/nano carbon black particles and to validate the experimental results by the results obtained representative volume element (RVE) models using finite element analysis. In this paper, the perfect adhesive bonding is assumed between matrix and the nanoparticle without interphase.

- *T.Prasad is currently pursuing Ph.D degree program in Mechanical Engineering in JNTU University, Hyderbad, India, Mobile-9989177045. E-mail: tatapudi.prasad@gmail.com*
- *A. Chennakesava Reddy is currently Proffsor and BOS Chairman, Department of Mechanical engineering, JNT University Hyderabad, India, Mobile-09440568776. E-mail: acreddy@jntuh.ac.in*

2 Strengthening Mechanisms

The strength of a particulate metal matrix composite depends on the strength of the weakest zone and metallurgical phenomena in it [9]. Even if numerous theories of composite strength have been published, none is universally taken over however. Along the path to the new criteria, we attempt to understand them.

For very strong particle-matrix interfacial bonding, Pukanszky et al. [10] presented an empirical relationship as given below:

$$\sigma_c = \left[\sigma_m \left(\frac{1-v_p}{1+2.5v_p}\right)\right] e^{Bv_p} \qquad (1)$$

where B is an empirical constant, which depends on the surface area of particles, particle density and interfacial bonding energy. The value of B varies between from 3.49 to 3.87. This criterion has taken care of the presence of particulates in the composite and interfacial bonding between the particle/matrix. The effect of particle size and voids/porosity were not considered in this criterion.

Considering adhesion, formation of precipitates, particle size, agglomeration, voids/porosity, obstacles to the dislocation, and the interfacial reaction of the particle/matrix, the formula [11] for the strength of composite is stated below:

$$\sigma_c = \left[\sigma_m \left\{\frac{1-(v_p+v_v)^{2/3}}{1-1.5(v_p+v_v)}\right\}\right] e^{m_p(v_p+v_v)} + kd_p^{-1/2} \qquad (2)$$

where, $k = E_m m_m / E_p m_p$; v_v and v_p are the volume fractions of voids/porosity and nanoparticles in the composite respectively, m_p and m_m are the possion's ratios of the nanoparticles and matrix respectively, d_p is the mean nanoparticle size (diameter) and E_m and E_p is elastic moduli of the matrix and the particle respectively. Elastic modulus (Young's modulus) is a measure of the stiffness of a material and is a quantity used to characterize materials. Elastic modulus is the same in all orientations for

isotropic materials. Anisotropy can be seen in many composites. Ishai and Cohen [12] developed based on a uniform stress applied at the boundary; the Young's modulus is given by

$$\frac{E_c}{E_m} = 1 + \frac{1+(\delta-1)v_p^{2/3}}{1+(\delta-1)(v_p^{2/3}-v_p)} \quad (3)$$

which is upper-bound equation. They assumed that the particle and matrix are in a state of macroscopically homogeneous and adhesion is perfect at the interface. The lower-bound equation is given by

$$\frac{E_c}{E_m} = 1 + \frac{v_p}{\delta/(\delta-1)-v_p^{1/3}} \quad (4)$$

Where, $\delta = E_p/E_m$.

The equation [11] to find Young's modulus including the effect of voids/porosity in the composite is given below:

$$\frac{E_c}{E_m} = \left(\frac{1-v_v^{2/3}}{1-v_v^{2/3}+v_v}\right) + \frac{1+(\delta-1)v_p^{2/3}}{1+(\delta-1)(v_p^{2/3}-v_p)} \quad (5)$$

where, $\delta = E_p/E_m$. E_c, E_m and E_p are the elastic moduli of composite, matrix and nanoparticles respectively.

3 Finite Element Numerical Modeling

The finite element procedure and analytical methods have been exceptionally effective in determining the mechanical properties of non-homogeneous materials like composites [13]. In finite element numerical models very fine meshes need to be applied inside and around the interphase layers which results in large number of degrees of freedom. Currently, the use of a representative volume element (RVE) or a unit cell [14] of the composite microstructure, in conjunction with a finite element (FE) analysis tool is well established for examining the effective material properties and understanding the micromechanics of the composite materials.

4 Materials and Methods

The matrix material was AA6061 aluminum alloy. The optical microstructure of AA6061 aluminum alloy is shown in figure 1(a). The reinforcement material was carbon nanoparticles of average size 100nm. The morphology of carbon nanoparticles was spherical, and they appear as a black powder (figure 1(b)).

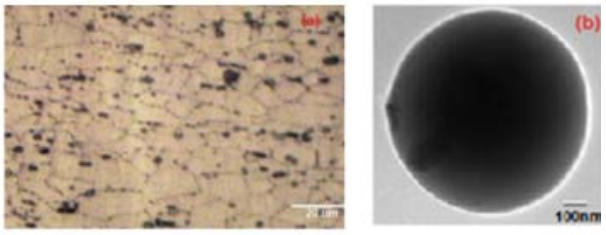

Fig. 1. Microstructure of (a) AA6061 and (b) carbon black nanoparticle.

4.1 Preparation of Composite Specimens

The matrix alloys and composites were prepared by the stir casting and low-pressure die casting process. The volume fractions of carbon black reinforcement were 10%, 20%, and 30%. AA6061 matrix alloy was melted in a resistance furnace. The crucibles were made of graphite. The melting losses of the alloy constituents were taken into account while preparing the charge. The charge was fluxed with coverall to prevent dressing. The molten alloy was degasified by tetrachlorethane (in solid form). The crucible was taken away from the furnace and treated with sodium modifier. Then the liquid melt was allowed to cool down just below the liquidus temperature to get the melt semi solid state. At this stage, the preheated (500^0C for 1 hour) reinforcement particles were added to the liquid melt. The molten alloy and reinforcement particles are thoroughly stirred manually for 15 minutes. After manual steering, the semi-solid, liquid melt was reheated, to a full liquid state in the resistance furnace followed by an automatic mechanical stirring using a mixer to make the melt homogenous for about 10 minutes at 200 rpm. The temperature of melted metal was measured using a dip type thermocouple. The preheated cast iron die was filled with dross-removed melt by the compressed (3.0 bar) argon gas [11].

4.2 Heat Treatment

Prior to the machining of composite samples, a solution treatment was applied at 500^0 C for 1 hour, followed by quenching in cold water. The samples were then naturally aged at room temperature for 100 hours.

4.3 Tensile Tests

The heat-treated samples were machined to get flat-rectangular specimens (figure 2) for the tensile tests. The tensile specimens were placed in the grips of a Universal Test Machine (UTM) at a specified grip separation and pulled until failure. The test speed was 2 mm/min (as for ASTM D3039). A strain gauge was used to determine elongation as shown in figure 3.

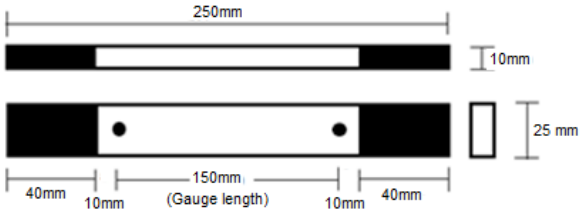

Fig. 2. Shape and dimensions of tensile specimen.

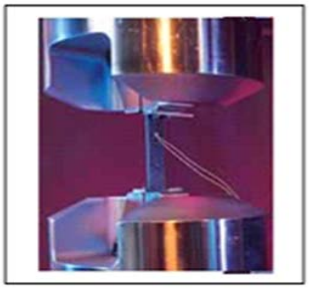

Fig. 3. Tensile testing.

4.4 Optical and SEM Analysis

An image analyzer was used to study the distribution of the reinforcement particles within the AA6061 aluminum alloy matrix. The polished specimens were ringed with distilled

water, and etched with 0.5% HF solution for optical microscopic analysis. Fracture surfaces of the deformed/fractured test samples were analyzed with a scanning electron microscope (SEM) to define the macroscopic fracture mode and to establish the microscopic mechanisms governing fracture. Samples for SEM observation were obtained from the tested specimens by sectioning parallel to the fracture surface and the scanning was carried using S-3000N Toshiba SEM.

4.5 RVE Modeling using Finite Element Analysis

The representative volume element (RVE or the unit cell) is the smallest volume over which a measurement can be made that will yield a value representative of the whole. In this research, a cubical RVE was implemented to analyze the tensile behavior AA6061/carbon black nanocomposites (figure 4). The determination of the RVE's dimensional conditions requires the establishment of a volumetric fraction of spherical nanoparticles in the composite. Hence, the weight fractions of the particles were converted to volume fractions. The volume fraction of a particle in the RVE Vp (RVE) is determined using equation:

$$v_p(\text{RVE}) = \frac{\text{Volume of nanoparticle}}{\text{Volume of RVE}} = \frac{16}{3} \times \left(\frac{r}{a}\right)^3 \qquad (6)$$

where, r represents the nanoparticle radius and a indicates the length of the cubical RVE. The volume fraction of the nanoparticles in the composite (v_p) was chosen to be 0.10, 0.20 and 0.30; the nanoparticle radius (r) was taken to be 100 nm.

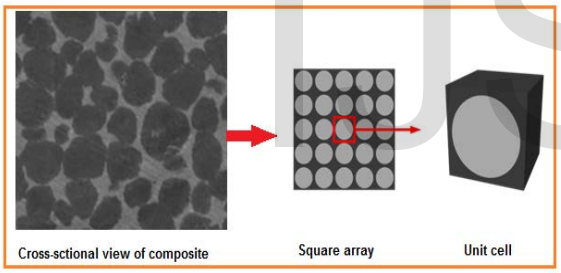

Fig. 4. The RVE model.

The RVE dimension (a) was determined by equalizing equation (6). The RVE scheme with adhesion (without interphase) was applied between the matrix and the filler. The loading on the RVE was defined as symmetric displacement, which provided equal displacements at both ends of the RVE. To obtain the nanocomposite modulus and yield strength, the force reaction was defined against displacement. The PLANE183 element was used in the matrix and the nanoparticle (table 1). In order to model the adhesion between the matrix and the particle, a COMBIN14 spring-damper element was used. The stiffness of this element was chosen to be unity, which determines the interfacial strength for the interface region.

To converge an exact nonlinear solution, it is also important to set the strain rates of the FEM models based on the experimental tensile tests' setups. Hence, FEM models of different RVEs with various particle contents should have comparable error values. In this respect, the ratio of the tensile test speed to the gauge length of the specimens should be equal to the corresponding ratio in the RVE displacement model. Therefore, the rate of displacement in the RVEs was set to be 0.1 (1/min).

TABLE 1

ELEMENTS FEATURES, APPLICATIONS AND SIZE RANGES USED IN RVE MODELING

Element code	Plane 183	Contact 172	Combination 14	Target 169
Feature	Quadrilateral-8 nodes	Linear 3 node	Longitudinal spring-damper	Shape complexity
Application	Matrix and nanoparticle	Interface contact	Elastic modeling of adhesion	Contact bodies

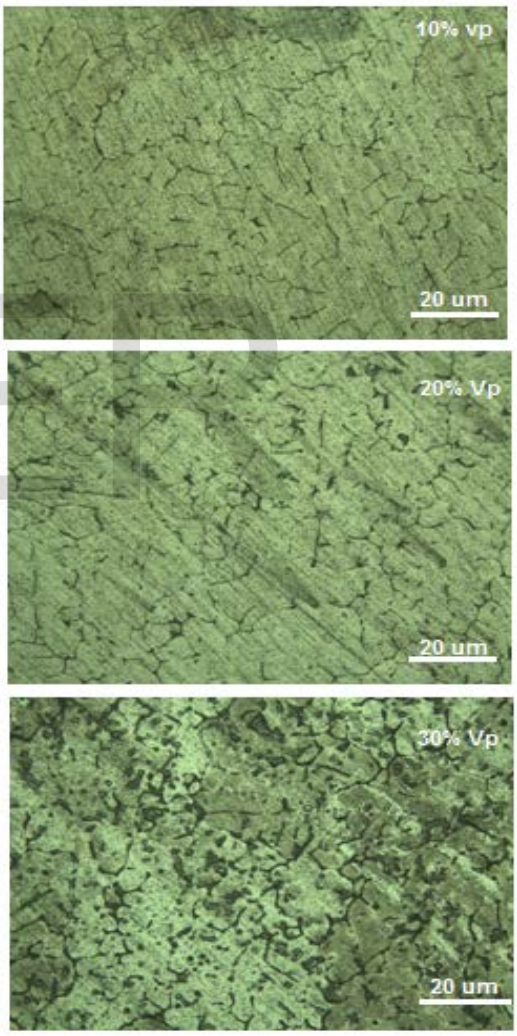

Fig.5. Optical microstructures of AA6061/carbon black nanocomposites.

5 RESULTS AND DISCUSSION

Figure 5 reveals the optical microstructure of AA6061/Carbon black nanocomposites. It is observed that the carbon black nanoparticles are randomly distributed in the AA6061 matrix. Figure 6 depicts the tensile strengths of the nanocomposites

obtained by FEA, Pukanszky et al model, AC Reddy model, and experimental procedure. The tensile strength increases with an increase of carbon black content in the nano campsites. The tensile strength (without voids) obtained by the finite element analysis (FEA) were lower than the experimental values. Pukanszky et al model did not include the effect of voids present in the nanocomposites. When voids were considered in the composites the interface region was stiffened (with good bonding between particle and matrix) and this caused the tensile strength to remain constant with an increase in the nanoparticles content. This was on account of the failure which was occurred in the regions of voids or in the matrix. The tensile strengths obtained by AC Reddy model (with voids) and experimental results were almost equal.

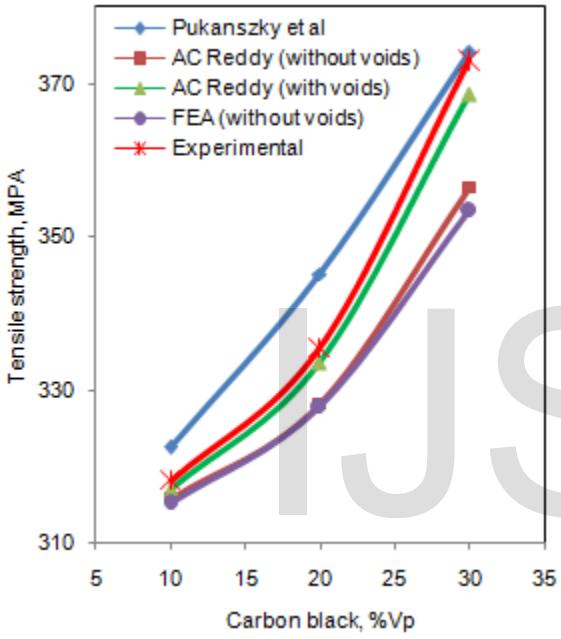

Fig. 6. Effect of volume fraction on tensile strength.

The adhesive bond was broken between the carbon black nanoparticle and AA6061 alloy matrix in the nanocomposite when the stress was exceeded the tensile strength (310 MPa) of the matrix as shown in figure 7. It is also observed form figure 7 that the load transfer from the matrix to the nanoparticle increases with increasing content of carbon black nanoparticles in the composite.

Figure 8 shows the elastic strain contours of the RVE models. According to figure 8, the RVE is expanded elastically away from the nanoparticle in the direction of the tensile loading. This increases the contact area between the particle and the matrix in the perpendicular direction to the tensile loading and decreases the contact area between the particle and the matrix in the direction of the tensile loading. In addition, the deformation is propagated in the normal direction to the tensile loading.

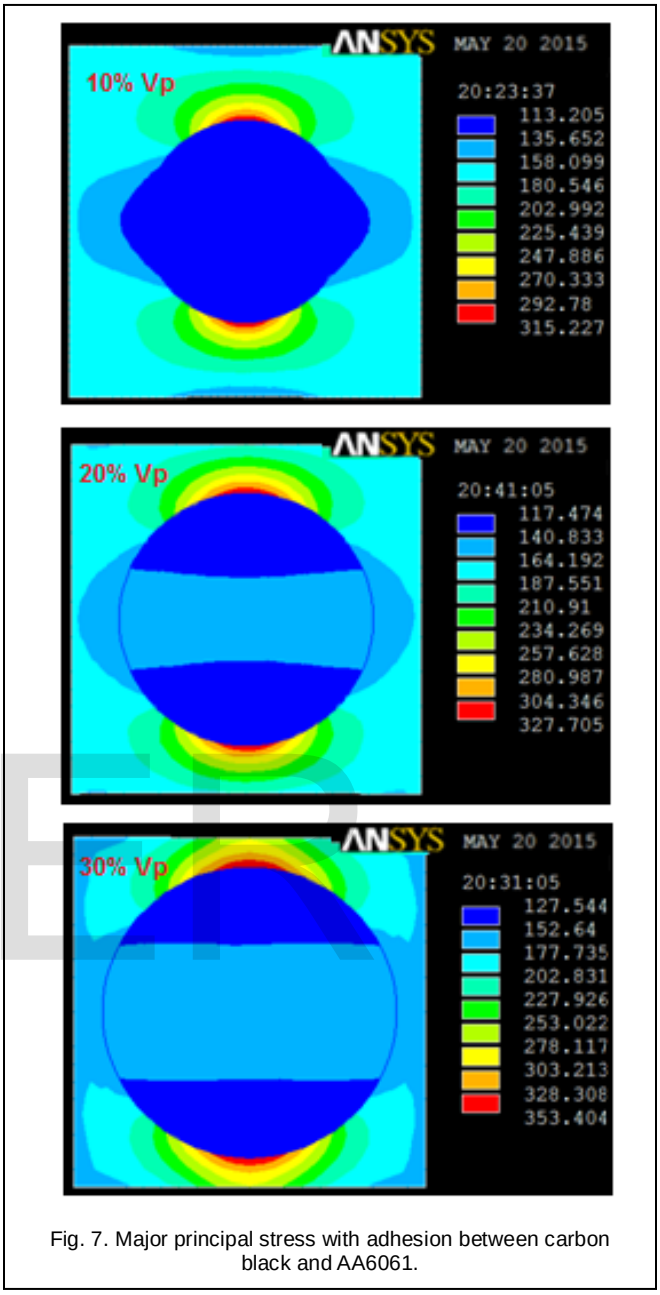

Fig. 7. Major principal stress with adhesion between carbon black and AA6061.

Figure 9 shows the variations of von Mises stress in the nanocomposites. The von Mises stress increases with an increase of carbon black content. It is observed that the interfacial debonding is high between the particle and the matrix because the local stress concentration around the nanoparticle increases with an increase in the volume fraction of carbon black in the nanocomposite.

Table 2 gives the elastic (tensile) moduli of the nanocomposites obtained by the Rule of Mixtures, FEA, Ishai and Cohen model and AC Reddy model with respect to the volume fraction of carbon black nanoparticles. By increasing the nanoparticles the elastic modulus increases appreciably. The results provided by FEA and AC Reddy model are closer than the results obtained by the Rule of Mixture and Ishai and Cohen model. This is due to the fact that the existence of voids in the

nanocomposites.

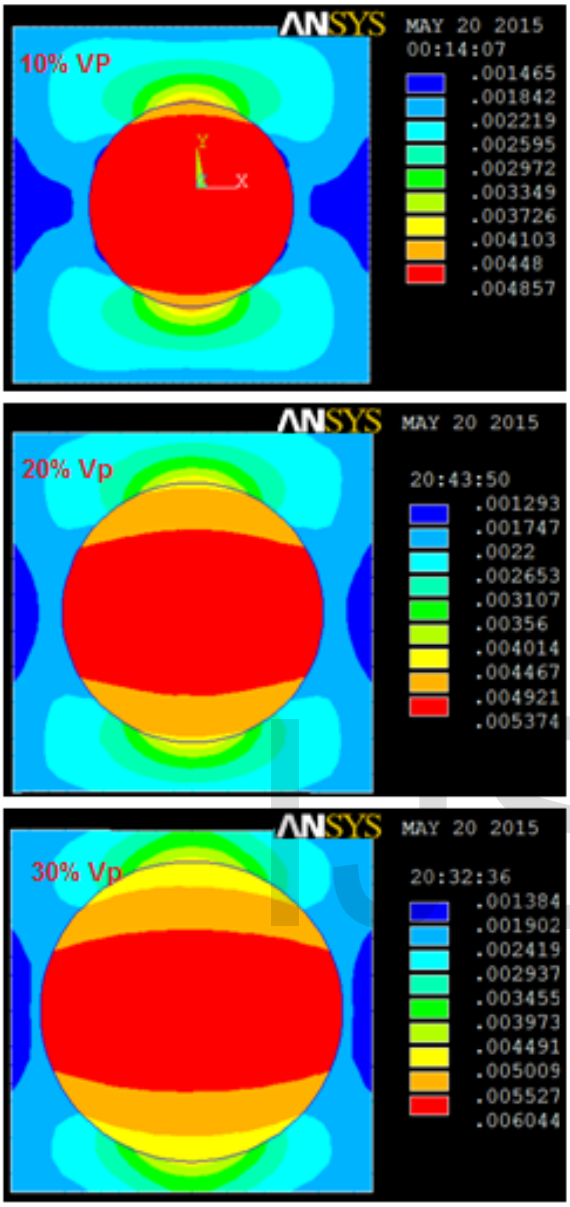

Fig. 8. Elastic strain in the direction of tensile loading.

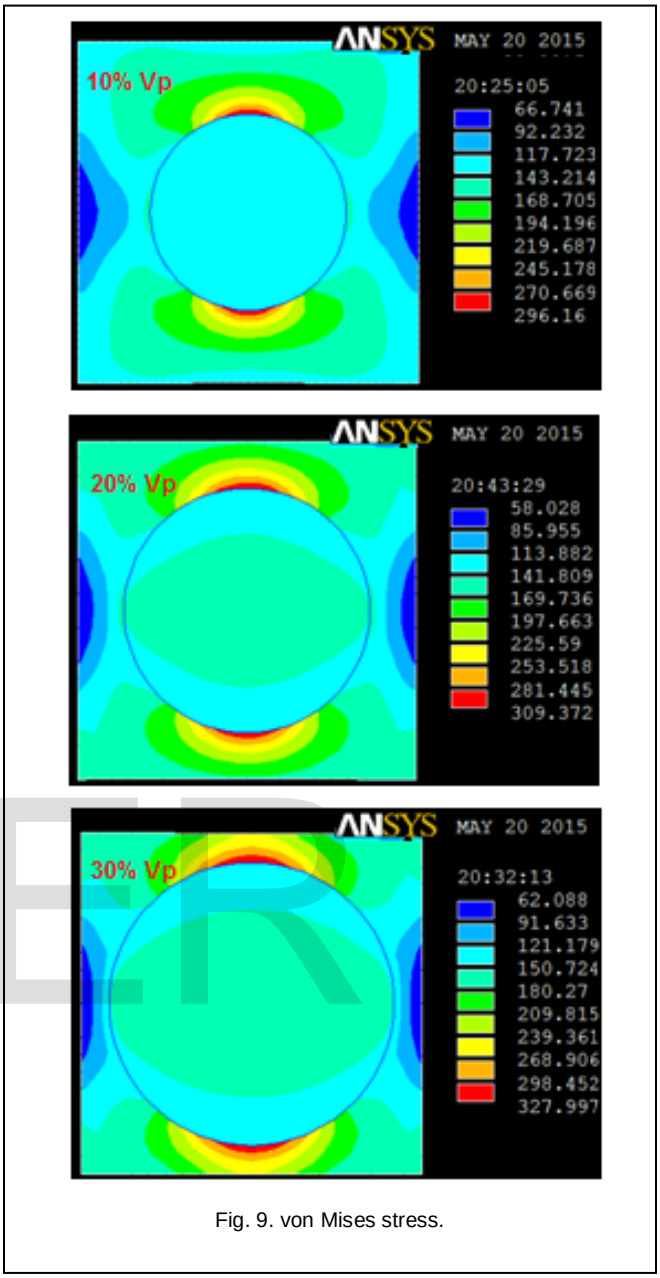

Fig. 9. von Mises stress.

6 Conclusion

The carbon black nanoparticles were randomly distributed in the AA6061 matrix. The tensile strength was increased with an increase of carbon black content in the nanocomposites. The adhesive bond was broken between the carbon black nanoparticle and AA6061 alloy matrix in the nanocomposite when the stress was exceeded the tensile strength (310 MPa) of the matrix. The RVE was expanded elastically away from the nanoparticle in the direction of the tensile loading. By increasing the nanoparticles the elastic modulus was increased appreciably.

TABLE 2
ELASTIC MODULUS OBTAINED FROM MODELS

Model	Elastic Modulus, GPa		
	10% Vp	20% Vp	30% Vp
Ishai and Cohen	169.90	177.34	184.78
Rule of Mixture	88.05	93.36	98.68
AC Reddy	168.43	175.38	182.31
FEA	168.04	175.06	181.98

Acknowledgment

The authors wish to thank University Grants Commission (UGC), New Delhi. This work was supported in part by a grant from UGC-SAP project.

REFERENCES

[1] A.Chennakesava Reddy, "Mechanical properties and fracture behavior of 6061/SiCp Metal Matrix Composites Fabricated by Low Pressure Die Casting Process," Journal of Manufacturing Technology Research, vol.1, no. 3/4, pp. 273-286, 2009.

[2] A.Chennakesava Reddy, Essa Zitoun, "Tensile properties and fracture behavior of 6061/Al_2O_3 metal matrix composites fabricated by low pressure die casting process," International Journal of Materials Sciences, vol.6, no.2, pp. 147-157, 2011.

[3] K. Friedrich , Z. Zhang , A.K. Schlarb, "Effects of various fillers on the sliding wear of polymer composites," Composites Science and Technology, vol. 65, pp.2329-2343, 2005.

[4] M. Romanowicz, "Progressive failure analysis of unidirectional fiber-reinforced polymers with inhomogeneous interphase and randomly distributed fibers under transverse tensile loading," Composites part A, vol. 41, pp.1829-1838, 2010.

[5] Y.S.Thio, A.S.Argon , R.E.Cohen , M.Weinberg , "Toughening of Isotactic Polypropylene with $CaCO_3$ Particles," Polymer, vol. 43, pp. 3661-3674, 2002.

[6] A. Chennakesava Reddy, "Analysis of the Relationship Between the Interface Structure and the Strength of Carbon-Aluminum Composites,"pp.61-62, NATCON-ME, Bangalore, 13-14th March, 2004.

[7] K. Wang, J. Wu, L. Ye, H. Zeng, "Mechanical properties and toughening mechanisms of polypropylene/barium sulfate composites," Composites: Part A, vol. 34, pp.1199-1205, 2003.

[8] A.Chennakesava Reddy, "Experimental evaluation of elastic lattice strains in the discontinuously SiC reinforced Al-alloy composites," National Conference on Emerging Trends in Mechanical Engineering, Nagapur, 05-06th February, VC-12, 2004.

[9] A.Chennakesava Reddy, "Influence of strain rate and temperature on superplastic behavior of sinter forged Al6061/SiC metal matrix composites," International Journal of Engineering Research & Technology, vol.4, no.2, pp. 189-198, 2011.

[10] B. Punkanszky, B.Turcsanyi, and F.Tudos, "Effect of interfacial interaction on the tensile yield stress of polymer composites", In: H. Ishida, editor, Interfaces in polymer, ceramic and metal matrix composites, Amsterdam: Elsevier, pp 467-7, 1988.

[11] A. Chennakesava Reddy, "Influence of Particle Size, Precipitates, Particle Cracking, Porosity and Clustering of Particles on Tensile Strength of 6061/SiCp Metal Matrix Composites and Validation Using FEA," International Journal of Material Sciences and Manufacturing Engineering, vol.42, no.1, pp. 1176-1186, 2015.

[12] O. Ishai, and I.J Cohen, "Elastic properties of filled and porous epoxy composites", International Journal of Mechanical Sciences, vol. 9, pp 539-546, 1967.

[13] A. Chennakesava Reddy, "Finite element analysis of elastic-plastic and tensile damage response in carbon-carbon composites under vechicular crush conditions," National Conference on Emerging Trends in Mechanical Engineering, Nagpur, 05-06th February, IIA-6, 2004.

[14] R. Hill, "Elastic properties of reinforced solids: some theoretical principles," Journal of the Mechanics and Physics of Solids, vol. 11, no.5, 1963.